International Journal of Nanomedicine

Dovepress

open access to scientific and medical research

Open Access Full Text Article

ORIGINAL RESEARCH

Graphdiyne Oxide-Mediated Photodynamic Therapy Boosts Enhancive T-Cell Immune Responses by Increasing Cellular Stiffness

Lejia Zhang*, Kuangwu Pan*, Siyuan Huang, Xiliu Zhang, Xinyu Zhu, Yi He, Xun Chen, Yuquan Tang, Lingyu Yuan, Dongsheng Yu

Hospital of Stomatology, Sun Yat-Sen University, Guangdong Provincial Key Laboratory of Stomatology, Guanghua School of Stomatology, Guangzhou, People's Republic of China

*These authors contributed equally to this work

Correspondence: Dongsheng Yu, Hospital of Stomatology, Sun Yat-Sen University, Guangdong Provincial Key Laboratory of Stomatology, Guanghua School of Stomatology, Guangzhou, People's Republic of China, Email yudsh@mail.sysu.edu.cn

Purpose: Nanomaterial-based photodynamic therapy (PDT) has been commonly used for the treatment of cancerous tumors. Despite significant achievements made in this field, the intrinsic impact of nanomaterials-based PDT on the mechanical properties of oral squamous cell carcinoma (OSCC) cells is not entirely understood. Here, we used atomic force microscopy (AFM) to measure the stiffness of OSCC cells subjected to PDT in co-culture systems to evaluate the T cell-mediated cancer cell-killing effects.

Methods: In this study, AFM was used to assess the stiffness of PDT-subjected cells. The phototoxicity of graphdiyne oxide (GDYO) was assessed using confocal laser scanning microscopy (CLSM), measurements of membrane cholesterol levels, and assessments of the F-actin cytoskeleton. A co-culture system was used to evaluate the effects of $CD8^+$ T cells (cytotoxic T lymphocytes), demonstrating how PDT modulates the mechanical properties of cancer cells and activates T cell responses. The antitumor immunotherapeutic effect of GDYO was further evaluated in a murine xenograft model.

Results: GDYO increased the mechanical stiffness of tumor cells and augmented T-cell cytotoxicity and inflammatory cytokine secretion (IFN-γ and TNF-α) under laser in vitro. Furthermore, GDYO-based PDT exerted inhibitory effects on OSCC models and elicited antitumor immune responses via specific cytotoxic T cells.

Conclusion: These results highlight that GDYO is a promising candidate for OSCC therapy, shifting the mechanical forces of OSCC cells and breaking through the barriers of the immunosuppressive tumor microenvironment. Our study provides a novel perspective on nanomaterial-based antitumor therapies.

Keywords: graphdiyne oxide, photodynamic therapy, stiffness, immunotherapy, cytotoxic T lymphocytes, oral squamous cell carcinoma cells

Introduction

OSCC is the most prevalent type of head and neck cancer leading to substantial morbidity and mortality.[1] Conventional treatment types such as surgical resection, radiotherapy, and chemotherapy,[2–4] can effectively treat early-stage tumors but are less effective for advanced and metastatic cancers.[5] In recent years, cancer immunotherapy has emerged as a new type of treatment for primary tumors, as activated immune cells can recognize and eradicate residual cancer cells, thereby reducing tumor metastasis and recurrence.[6–8] Therefore, this type of therapy has proven highly successful in clinical practice. However, some malignancies rely on immune checkpoints, such as cytotoxic T-lymphocyte-associated protein 4 (CTLA4) and programmed cell death protein 1 (PD-1)/programmed cell death-ligand 1 (PD-L1),[9,10] which are used by tumors to escape immune surveillance. In recent years, the emergence of immune checkpoint blockade (ICB) has shifted the paradigm in clinical oncology, as the approach can destroy tumor immune tolerance, stimulate T lymphocytes to attack tumor cells,

Received: 18 October 2022
Accepted: 14 January 2023
Published: 15 February 2023

Graphical Abstract

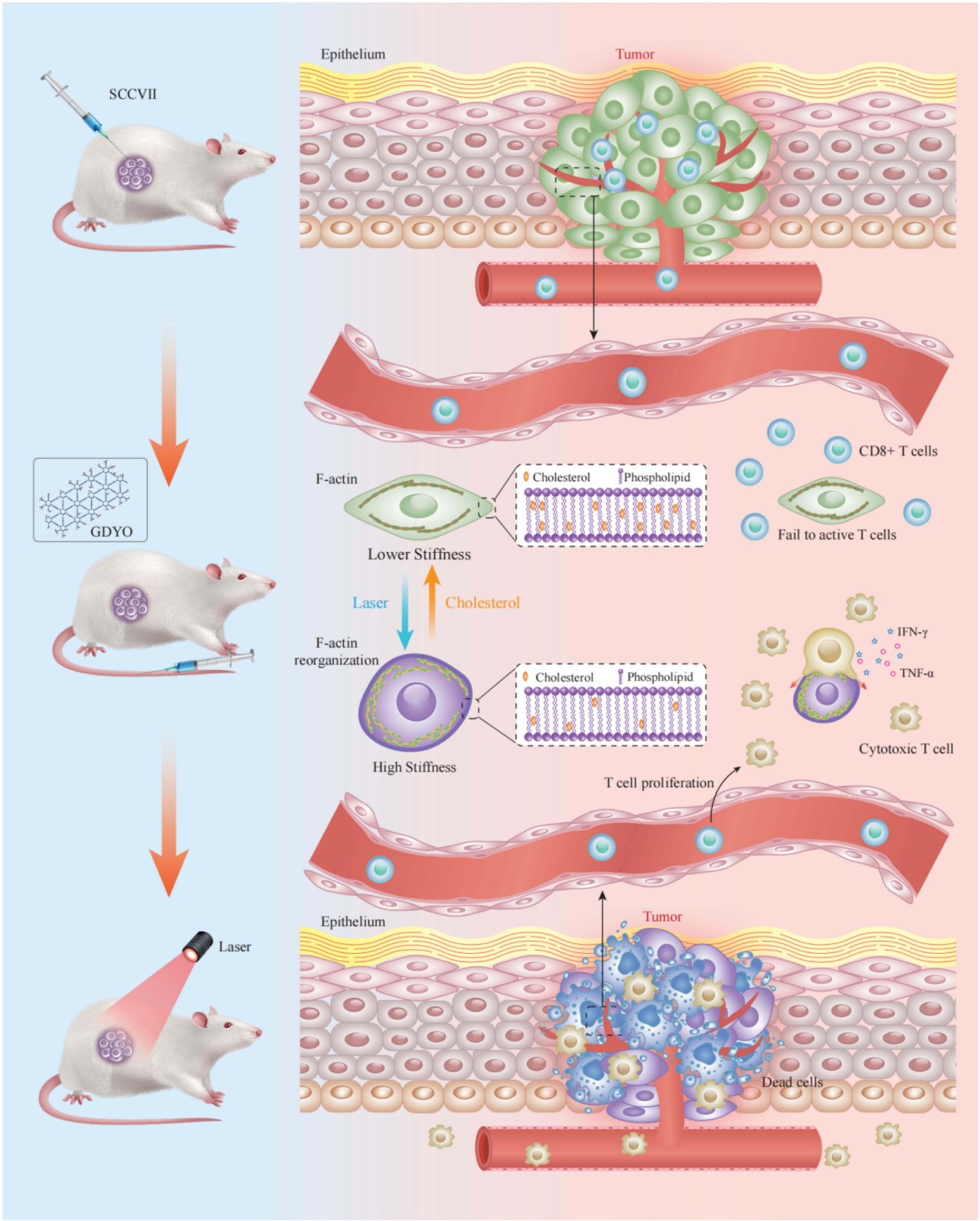

and has a durable clinical effect. This therapy type has improved the prognosis of various cancers. However, a large number of patients still do not respond to available immune checkpoint inhibitors,[11] which limits the clinical efficacy of this approach. Of note, tumors tend to stimulate immunosuppressive pathways, and therefore developing new ways of breaking immunosuppression is of crucial importance. Although efforts have been made to identify new immune checkpoints based on biochemical signals,[12,13] current research efforts are not typically focused on biomechanical signals.

Stiffness is a fundamental biomechanical feature of cells. Accumulating evidence suggests that cancer cells are relatively softer and more plastic than normal cells,[14,15] indicating that cancer cells have a lower Young's modulus. Low cell stiffness is associated with cancer cell adhesion, metastatic potential, and invasiveness.[16,17] Hence, the stiffness of cancer cells is associated with malignant transformation and tumor progression. It is well recognized that the mechanical properties of tumors influence their physical interactions with T cells and that increased cancer-cell stiffening triggers stronger T-cell-derived cytotoxicity.[18] Mechanical softness in turn affects mechanics-mediated tumor immune evasion. Therefore, strengthening the cellular stiffness of cancer cells to increase the efficacy of immunotherapies is a promising therapeutic approach in oncology.

PDT, as a non-invasive therapeutic approach, relies on the introduction of a photosensitizer into the tumor tissue and the delivery of light with a specific wavelength, with subsequent activation of the photosensitizer and in situ generations of several reactive oxygen species (ROS) to destroy cancer cells,[19] not only to directly exert a cytotoxic killing effect but also to induce immunogenic cell death (ICD).[20] However, the immunosuppressive properties of the tumor microenvironment (TME) greatly limit the efficacy of PDT. Therefore, it has recently been used in combination with immune checkpoint inhibitors as an adjuvant therapy for immune stimulation with a goal to reverse the immunosuppressive microenvironment (ITM) and restart T cell immune activation. Still, checkpoint inhibitors may have several limitations including a new type of side effect, termed as immune related adverse events (IRAEs), limited tumor penetration, and insufficient pharmacokinetics.[21] Therefore, the efficiency of this approach needs to be improved for better clinical outcomes.

GDYO, an emerging carbon nanozyme, has catalase-like activity, and is characterized by a unique planar structure. Specifically, it contains a combination of sp and sp^2 hybridized carbon atoms, and a network of benzene rings conjugated by alkyne bonds, which result in a homogeneous distribution of nanopores, an easily tunable electronic structure and a large conjugated system.[22,23] Due to its unique physical structure and excellent chemical properties,[24] GDYO might be highly useful in the biomedical field,[21] eg in the development of multifunctional nanoplatforms. In this regard, GDYO has physicochemical features of a 2D nanomaterial, which resemble those of black phosphorus, 2D Ti nanosheets (NSs), MXenes and their derivatives,[25–29] all of which have been widely used in phototherapy, including photothermal therapy (PTT) and PDT, targeted drug delivery, biosensor construction, and other antibacterial and anticancer studies. Currently, GDYO is a good candidate as a photoinitiator in phototherapy,[30,31] and could also be beneficial for immune cell activation.[32,33] However, much attention has been devoted to eliminating cancer cells via attacking lysosomes, plasma, membranes, mitochondria, and other subcellular targets,[34] and it is unclear how intrinsically nanomaterial-based PDT could impact the mechanical properties of intractable tumor cells.

In this study, we discovered that the stiffness of OSCC cells was enhanced by GDYO-based PDT, following altered membrane cholesterol levels and F-actin cytoskeleton organization. Further experiments revealed that mechanical changes rendered cancer cells more vulnerable to cytotoxic T lymphocytes (CTLs) in a co-culture model of SCC9 cells and T cells, suggesting that immunosurveillance is linked to mechanical tissue properties. These findings provide a theoretical basis for the development of nanomaterial PDT treatments in OSCC.

Materials and Methods

Preparation and Characterization of GDYO

Oxidation of GDY (XFNANO, Nanjing, China) resulted in the formation of GDYO. A mixture of H_2O_2 and H_2SO_4 was used as a complex oxidant. GDY (50 mg) was gradually incorporated into a solution of 30% H_2O_2 (1 mL) and 98% H_2SO_4 (2.5 mL) for one hour while submerged in freezing water. By adding 50 mL of double-distilled water and then using a dialysis membrane (MWCO=3500) for seven days to remove the mixed acid, oxidization was stopped, and the GDYO was obtained by sonication for 4 h in water. Subsequently, it was dried under vacuum. AFM and transmission electron

microscopy (TEM) were employed to analyze the morphology of GDYO. X-ray photoelectron spectroscopy (XPS) spectra were obtained using an X-ray photoelectron spectroscopy device. Raman spectroscopy was used to analyze the chemical structure and assess the quality and uniformity of GDYO. Fourier-transform infrared (FT-IR) spectroscopy was used to investigate the hydrophilic and surface functional groups.

In vitro Cell Cytotoxicity and Cell Uptake

The human oral squamous cell carcinoma cell lines SCC9 and human oral keratinocyte (HOK) were purchased from the ATCC. To determine the biosafety of GDYO, normal oral keratinocyte (NOK) cells were added to 96-cell plates and cultured for 24 h, and fresh GDYO medium was subsequently added to wells at different concentrations. Twelve h later, viable cells were detected using the Cell Counting Kit-8 assay (CCK-8). For the tracking of cellular uptake, The SCC9s were seeded on 20 mm confocal dishes and grown in a humidified environment (37 °C, 5% CO_2) using RPMI-1640 media containing 10% fetal bovine serum (FBS). After 24 h of incubation, the cells were treated with GDYO at a concentration of 50 μg/mL for 6 h, following washing with PBS and staining with DAPI. The cells were imaged using a fluorescence microscope.

In vitro Photodynamic Assays

The SCC9 cells were seeded in a 24-well culture plate at a density of 3×10^4 cells per well, and after 24 h, they were incubated with GDYO at different concentrations for another 12 h. The cells were then exposed to laser radiation for five minutes. Following incubation for another 24 h, cell viability and apoptotic cells were analyzed in a CCK-8 assay and by using a calcein-AM/PI kit, respectively.

Measurement of Cell Cortical Stiffness by AFM

AFM images were acquired using Dimension Fastscan with a ScanAsystTM AFM (Bruker, Santa Barbara, CA). None of the cells used in the AFM assay were fixed, and the morphological images and Young's modulus of the cells treated under different conditions were recorded simultaneously within one hour of treatment. Following the acquisition of AFM images, the marking location on the glass slide was examined using an optical microscope (Leica_DM2500B, Germany) equipped with a 100X objective lens, and photographs were obtained using a digital camera system at a resolution of 1360×1024 pixels, and the force curves obtained were processed. Finally, the Young's modulus of cancer cells was determined using the Nanoscope software (Bruker).

Membrane Lipid Raft Structure and F-Actin Determination

SCC9 cells were seeded in a 24-well plate at a concentration of 1×10^5 cells per well, and the cells were then grown for 24 h. The medium was removed and the following conditions were applied to observe the membrane lipid raft variation: (1) PBS, (2) laser, (3) GDYO (25 μg/mL), (4) M-β-CD (5 mM), (5) GDYO + laser. After the treatment, culture media were discarded, the cells were washed with PBS three times, and 1 mL of AF488-CTB (5 μg/mL) was added to each well. Following three PBS rinses, the cells were fixed with 1 mL of 4% paraformaldehyde for 15 min, and 1 mL DAPI was added for nuclear staining (15 min, 37 °C), followed by three PBS washes and photographed with a confocal laser microscope. To obtain F-actin fluorescence images, SCC9 cells treated as described above were divided into four groups as follows: (1) PBS, (2) laser, (3) GDYO, (4) GDYO + laser, and stained with phalloidin-iFluor 488 and DAPI for 30 min.

In vitro Co-Culture System and Killing Assays of Cancer Cells

Single-cell suspensions were extracted from the spleens of 6-week-old C57BL/6 mice to isolate $CD8^+$ T-cells. $CD8^+$ T cells were purified using a mouse $CD8^+$ isolation kit (Stemcell, Canada). Then, the harvested $CD8^+$ T cells were seeded at a density of 1×10^5 in 96-well plates and supplemented with anti-CD28 (1 μg/mL; BioLegend), anti-CD3 (5 μg/mL; Biolegend), and IL-2 (40 U/mL) for 3 d to induce $CD8^+$ T cell activation. SCC9 cells, given the different treatments (PBS, GDYO, cholesterol, GDYO + L + Cholesterol, GDYO + L), were co-cultured for 5 hours with activated T cells at various ratios of effector to target. Using a Cyto Tox 96 Non-Radioactive Cytotoxicity Assay kit (Beyotime, China), the supernatant from each well was used for a lactate dehydrogenase cytotoxicity assay to measure target cell mortality, according to the manufacturer's recommended protocol. In other experiments, activated $CD8^+$ T cells were added at the

effector to target ratios of 10:1 for 5 h to quantify the death of cancer cells by flow cytometry, and then co-culture media were measured for the inflammatory mediators, including IFN-γ and TNF-α, using enzyme-linked immunosorbent assay (ELISA) kits (Thermo Fisher Scientific, USA).

Histological Analyses

Mouse tumors were sectioned and stained for immunofluorescence. After staining, images were obtained using a confocal microscope. Subcutaneous tumors collected from C3H mice were embedded with OCT, frozen for cryosections, and stained with filipin III (Guyan, Shanghai, China) at room temperature, and rinsed with PBS to determine the tumor cholesterol levels. The images were acquired using a confocal microscope.

Tumor Suppression and Immune Response in vivo

To establish an oral squamous cell carcinoma animal model, wild-type 6-to 8-week-old female C3H mice procured from Vital River Laboratory Animal Technology (Beijing, China) were subcutaneously injected with 3×10^6 SCCVII cells in the right armpit. The murine SCC cell line SCCVII was provided by Professor Yixiang Wang, Peking university school of stomatology. The 25 mice were randomly divided into five groups (5 animals per group), followed by intravenous injection of 1× PBS (200 μL) for groups (a) and (b), cholesterol for group (c), and GDYO (200 μL, 1 mg/mL) for groups (d) and (e). In group (e), intratumoral injections of cholesterol (2 mg per mouse) were administered to post-PDT animals every other day until their sacrifice. During treatment, the tumor area ((length × width^2)/2) and body weight were monitored every two days.

The mice were euthanized, and the tumors were fixed for immunofluorescence. Tumors and draining lymph nodes (DLNs) were isolated from all five groups and prepared as single-cell suspensions using digestive enzymes. Cells were stained with fluorescence-labeled anti-CD45, anti-CD3, anti-CD8, anti-IFN-γ and anti-TNF-α antibodies (eBioscience, USA), and dendritic cells (DCs) were tagged with anti-F4/80, anti-CD11c, anti-CD80, and anti-CD86 antibodies (eBioscience, USA), and then subjected to flow cytometry.[35] The Institutional Animal Care and Use Committee (IACUC) at Sun Yat-Sen University (Approval Number: SYSU-IACUC-2020-00042) reviewed and approved the animal use for these experiments, and all of the animal procedures were conducted in accordance with the Guidelines for the Care and Use of Laboratory Animals.

Statistical Analysis

All data are expressed as mean ± standard deviation (SD). Data graphs were obtained using Prism 8.0. $P < 0.05$ was considered statistically significant.

Results and Discussion

GDYO Characterization

As a novel material, the synthesis of GDYO was mainly performed by the acid-oxidation treatment. There are two main acid-oxidation ways to produce GDYO: the conventional Hummers' method and the modified Hummers' method. In the conventional Hummers' method, the widely used acid was a mixture of H_2SO_4 and $KMnO_4$. Compared with the conventional Hummers' method, The distinctive feature of the modified Hummers method is the choice of different oxidants, such as the possibility to change the ratio of the H_2SO_4/H_2O_2 mixture or to replace part of H_2SO_4 with HNO_3 as an electrolyte. GDYO used in this research was produced via a modified Hummers' method.[36–38] The morphological features of GDYO were determined in AFM images, and we found that the average height of GDYO was 3.5 nm (Figure 1A). TEM suggested that GDYO displays a nanosheet-like morphology (Figure 1B). The XPS (Figure 1C and Figure 1) spectrum of the GDYO nanosheet shows a peak at 284.4 eV, which corresponds to the binding energy of the C 1s orbital, and four subpeaks of C 1s at 284.5, 285.2, 286.4, and 288.4 eV, which are attributed to the orbitals of C═C (sp^2), C≡C (sp), C–O, and C═O bonds, respectively, implying the effective linkage of the benzene ring and two acetylenic linkages. The Raman spectrum of GDYO is shown in Figure 1E, with prominent peaks D and G at 1371 cm^{-1} and 1560 cm^{-1}, respectively, corresponding to carbon materials. The FTIR spectrum of GDYO shows a peak at 1506 cm^{-1} ascribed to the benzene ring; a peak at 1642 cm^{-1} ascribed to C═O stretching vibration; and a peak at 2098 cm^{-1} ascribed to C≡C stretching vibration (Figure 1F).

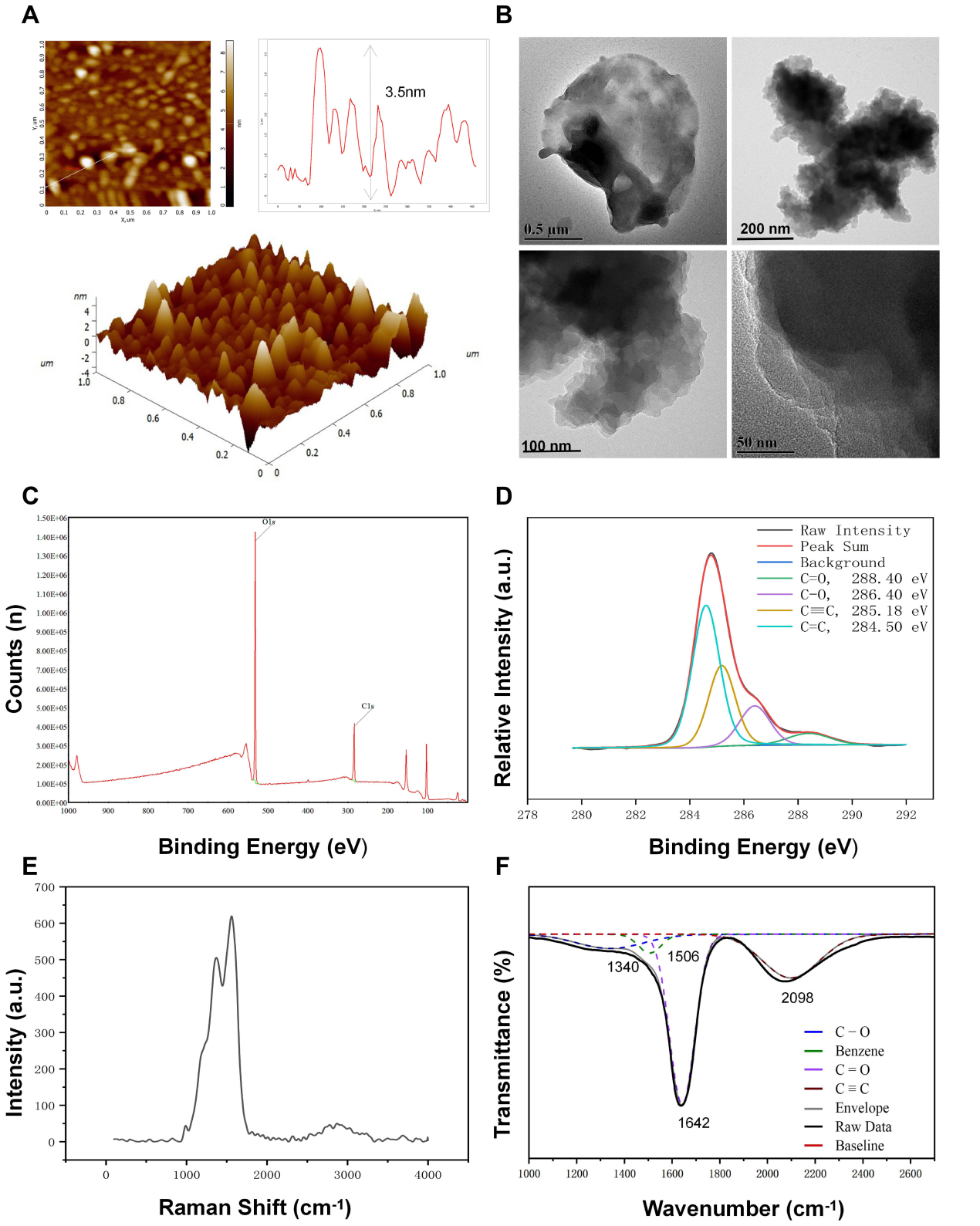

Figure 1 Physicochemical characterization of GDYO. (**A**) AFM images of GDYO. (**B**) TEM images of GDYO. (**C**) XPS survey scan and (**D**) C 1s spectra of GDYO. (**E**) Raman spectra of GDYO. (**F**) FTIR spectra of GDYO.

Photodynamic Efficacy of GDYO in vitro

For in vitro treatments, a CCK-8 assay was performed to examine the cytotoxicity of GDYO. As shown in Figure 2C, GDYO exhibited no significant cytotoxicity toward NOK cells, even when the concentration of GDYO reached 100 μg/mL, demonstrating the good biocompatibility of GDYO, consistently with previous results. Therefore, it can be assumed that GDYO has some advantages in biological applications, owing to its superior biocompatibility and low toxicity. In contrast, upon laser irradiation, the viability of SCC9 cells showed obvious dose-dependent PDT efficiency along with an increase in the concentration of GDYO (10 ug/mL-150 ug/mL). The cell viability decreased from 89% to 37.4%, highlighting its excellent performance as

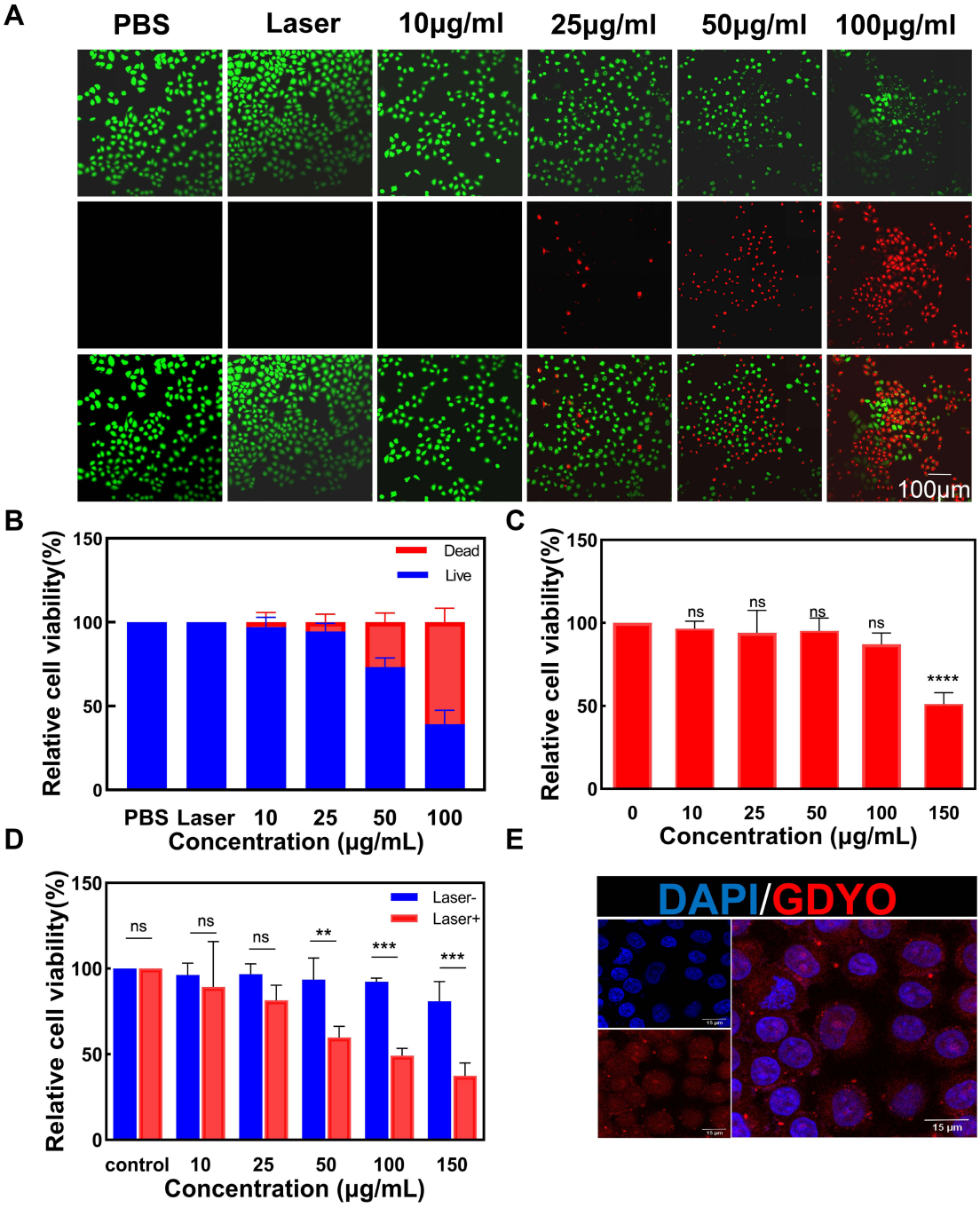

Figure 2 In vitro anticancer efficacy. (**A**) Antitumor effects of GDYO-PDT in SCC9 cells stained with PI (red, dead cells) and calcein AM (green, live cells), respectively. Fluorescent images were obtained by fluorescence microscopy. Scale bar = 100 nm. (**B**) Relative fluorescence quantitative analysis of live/dead fluorescence microscopy. (**C**) Cell viability of GDYO at different concentrations in the NOK normal cell line. **(D)** Cell viability of SCC9 cells incubated with GDYO at different concentrations under irradiation. (**E**) Confocal microscopic images of SCC9 cells after exposure to GDYO for 6 h. Scale bar = 15 μm. **P <0.01, ***P <0.001, ****P <0.0001.

a photodynamic agent, and the laser alone showed no harm to cancer cells. Notably, when the concentration of GDYO was as low as 25 μg/mL, approximately 81% of the cancer cells remained alive (Figure 2D). Remarkably, a live/dead cell staining assay was employed to further examine the photodynamic effect on SCC9 cells, in which green fluorescence represents live cells and red fluorescence represents dead or late apoptotic cells (Figure 2A and Figure 2). The control and laser groups showed only a few dead cells, and GDYO with laser resulted in the highest number of dead cells, which is consistent with the cytotoxicity assay. Therefore, GDYO can directly kill SCC9 cells through its photodynamic effects. Interestingly, the targeting ability of GDYO was detected, and red fluorescence of GDYO was clearly observed for 6 h, indicating that GDYO had specific targeting and accumulation in cancer cells (Figure 2E). Several nanomaterials have excellent photodynamic effects, among which GDYO and black phosphorus are structurally similar and possess a unique combination of properties such as ultra-high surface area, absence of toxic metal elements, adjustable band gap, biocompatibility, excellent biosafety, and broad absorption in the ultraviolet (UV)-visible and near-infrared (NIR) regions,[29,39,40] conferring efficient drug loading rate and photothermal conversion efficiency of GDYO. These synergistic effects greatly support the clinical application of GDYO.

Cellular Biomechanical Changes of Cancer Cells

The stiffness of cancer cells can be used to evaluate their adhesion, invasion, and metabolic states. Alterations in cancer cell stiffness are essential for antitumor responses of immune cells and immune evasion, and stiffer tumor cells are more sensitive to T cell killing. Therefore, we examined the impact of GDYO-based PDT on biomechanical properties. We directly used AFM to characterize the difference in stiffness and measure the morphological and biomechanical properties of GDYO in SCC9 cells after PDT in the non-killing state. As presented in Figure 3A, contact mode AFM showed that the control cells were spindle-shaped and had no obvious stress fibers, but the PDT-treated cells showed a distinct round shape and had visible cytoskeletal fibers around the nucleus (Figure 3B). The Young's modulus values of each group were calculated using the force-separation curve (n=12~14) (Figure 3C and Figure 3). We found that the mean Young's modulus increased from 1.25 Kpa to 3.21 Kpa after PDT treatment

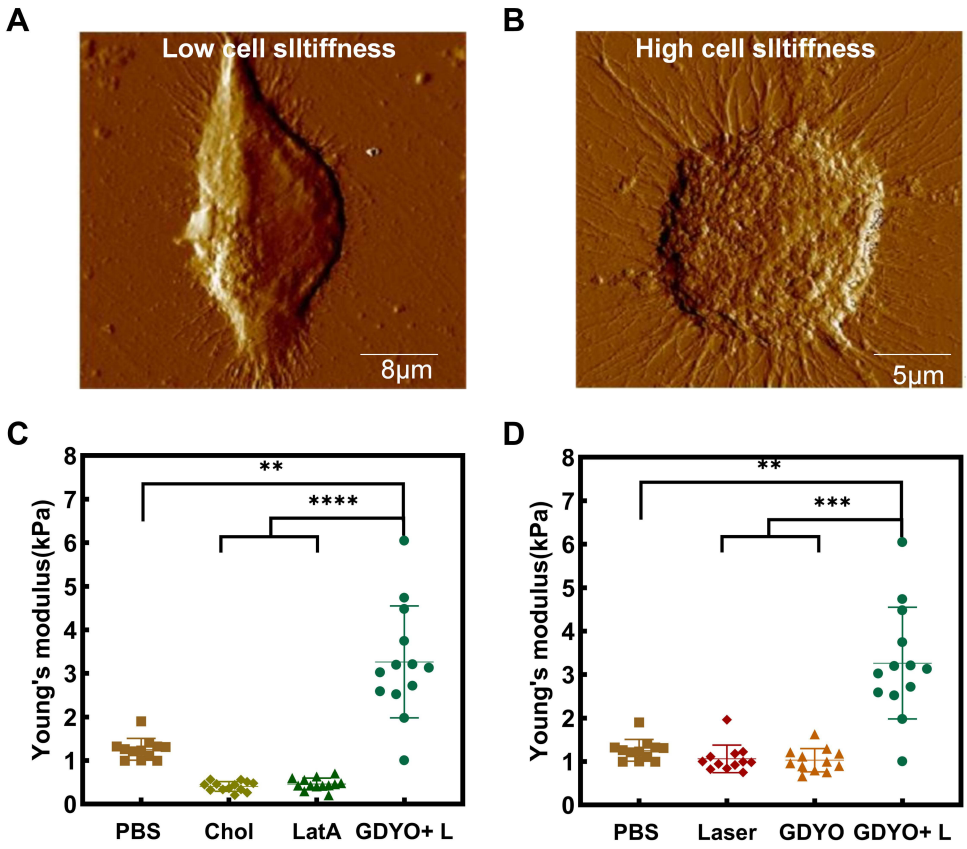

Figure 3 GDYO-based PDT enhances cells stiffness and modulates cellular morphology. (**A**) Morphological features of contact-mode AFM observed in the control (**B**) and SCC9 cells treated with the GDYO and laser. (**C**) and (**D**) Relative stiffness determined by quantitative analysis of the Young' s modulus of cells.**P <0.01, ***P <0.001, ****P <0.0001.

compared with the untreated cells. The results indicated that the GDYO-mediated group was significantly stiffer than the untreated group, and we found that cholesterol-supplemented tumor cells or cells pre-treated with cytoskeleton inhibitors, 2 μM Latrunculin A (LatA, Calbiochem, Merck) for 10 min, exhibited lower cortical stiffness than the untreated cells. Previous studies suggested that the change of cancer cell stiffness is directly associated with the underlying F-actin cytoskeleton and plasma membrane.[41,42] In traditional PDT, increased oxidative stress damages the cell membrane structure and reduces the elastic modulus of the cell membrane. However, HeLa cells that underwent PDT showed a higher Young's modulus and a larger redistribution in the F-actin network,[43] and it has been reported that an increase in ROS within a certain range leads to an increase in the Young's modulus of the cell membrane.[44] The photosensitizer-mediated PDT with CAT activity can effectively increase the elastic modulus of the cell membrane by removing ROS in time and can effectively inhibit the decreasion of Young's modulus due to oxidative stress injury by exogenous H_2O_2. GDYO is a new two-dimensional carbon nanomaterial with sp^2 and sp-hybridized carbon atoms, and its oxygen-containing group determines its catalase activity. Therefore, we speculate that GDYO, exhibiting CAT activity and peroxidase-like activity,[38] is a potential photosensitizer that enhances the mechanical properties of nanomaterial-based PDT of tumor cells.

Growing evidence suggests that cholesterol is an essential component of biological membranes and a key molecule in controlling changes in the membrane.[45] Cholesterol content also plays regulatory functions in prevent cancer cell invasion[46] and the immune response of cells by regulating the bending rigidity of cell membranes,[47] and this might be due to the depletion of cholesterol-enriched nanoscale membrane microdomains,[48] known as the lipid rafts. These cholesterol-enriched nanoscale membrane microdomains are commonly measured by cholera toxin B (CTB), which attaches to cells by binding to ganglioside GM1, the depletion or accumulation of which is directly correlated with membrane cholesterol content. SCC9 cells post-PDT or MeβCD treatment (used to deplete membrane cholesterol to increase stiffness) were stained with Alexa Fluor 488-conjugated CTB and observed by confocal microscopy. As shown in Figure 4A, only faint green fluorescence was observed in the PDT or MeβCD groups, compared to the control group with strong green fluorescence. These findings indicate that GDYO-PDT can affect the cholesterol formation in lipid rafts, which can be attributed to the ability of graphdiyne oxide-like materials to extract cholesterol from cell membranes.[49,50]

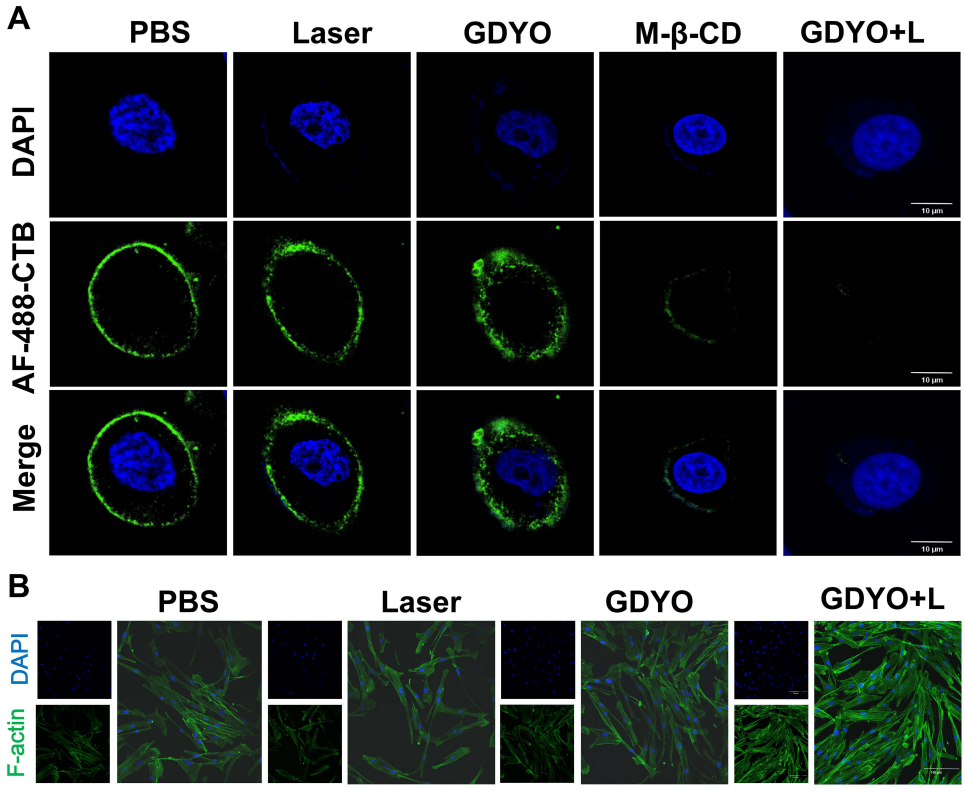

Figure 4 Membrane lipid rafts and F-actin of cancer cells. (**A**) AF488-CTB-tagged membrane lipid rafts and DAPI-stained nucleus were visible to CLSM, scale bar = 20 μm. (**B**) SCC9 cells show an increased F-actin polymerization as shown in the fluorescence images. Scale = 15 μm.

F-actin, as part of the cytoskeleton, partly contributes to the mechanical characteristics of cells, and its alteration affects cell stiffness. We then treated cancer cells with GDYO and laser combined to investigate the effect of PDT on the cytoskeleton. In concert with the AFM results, we observed the reorganization of microfilaments by confocal microscopy. F-actin filaments were observed in a fine network of untreated control cells (Figure 4B). In contrast, the photosensitized cells exhibited increased F-actin polymerization, as shown by the increase in fluorescence intensity. We hypothesized that the intensity of these F-actin alterations is affected by the light dose, type, concentration of the photosensitizer, and post-irradiation duration.[43,51]

Cancer-Cell Stiffness Improves T-Cell-Mediated Cytotoxicity

Infiltrating cytotoxic $CD8^+$ T cells play an essential role in anti-cancer immunosurveillance. To evaluate the cancer cell stiffness-elicited immune response of OSCC cells, we further investigated whether PDT-elicited tumor cell stiffness breaks the resistance to $CD8^+$ T cell-mediated cytotoxicity and induces stronger $CD8^+$ T cell activation in vitro, as the cytotoxic T lymphocyte ability could be confirmed in a SCC9 cells and T lymphocytes co-culture system. Activated $CD8^+$ cells were used as effector cells and co-incubated with pretreated SCC9 cells, which were used as target cells (Figure 5A). Cancer-cell mechanical properties are partly determined by membrane cholesterol, which affects target cell lysis,[52,53] Hence, before establishing the co-culture model, SCC9 cells were pre-treated with cholesterol. Subsequently, target cell lysis was measured by the release of lactate dehydrogenase,[6] and the tumor cell lysis efficiency increased significantly with PDT treatment. PDT enhances the cleavage of SCC9 cells by T cells. On the other hand, when supplemented with cholesterol, the survival rate of SCC9 cancer cells post-PDT was lower compared with the PBS group but showed a higher rate compared to the PDT group. There was no significant LDH release in the cholesterol + CTL, GDYO + CTL, or CTL groups (Figure 5B). Flow cytometry analysis also demonstrated that, when exposed to PDT treatment, toxin-induced cancer-cell apoptosis (34.6%, late and early apoptosis combined; gate Q2+Q3; Figure 5C) was increased at an effector cell-to-target cell ratio of 10:1, which was in accordance with the LDH release assay (Figure 5B). These results suggest that GDYO-based PDT efficiently improves T-cell-mediated cytotoxicity via modulating cancer cell stiffness.

The cytotoxic activity of T cells also generates different types of cytotoxic cytokines such as IFN-γ and TNF-α,[54] which are characteristic markers of T cell activation. The cytokine level in $CD8^+$ T cells suspensions after various treatments were determined using an ELISA kit. Production of these cytokines in the GDYO + laser group was markedly enhanced compared to that in the other groups co-cultured with cancer cells (Figure 5D and Figure 5). These results demonstrated that cell stiffness-enhanced phototherapy with GDYO could induce the proliferation and cytotoxic phenotype of T cells.

In vivo Photodynamic Efficacy of GDYO

We further evaluated the efficacy of GDYO in enhancing the immune response after treatment with mild PDT using an in vivo tumor model (Figure 6A). SCCVII tumor-bearing mice[55] were randomized into five groups (n=5) on day 7, namely PBS, laser, cholesterol, GDYO + laser and GDYO + laser + cholesterol. The mice were evaluated once every other day on three consecutive occasions. Upon irradiation, the tumor growth was slightly restrained with a mean volume of 800 mm^3, which was smaller compared to that of the PBS group (≈) and cholesterol group (≈991 mm^3); however, these antitumor effects were far less ($p < 0.001$) than those triggered by GDYO combined with light exposure. The GDYO + laser group was characterized by greatly suppressed tumor growth with a mean tumor volume of 405 mm^3, which was 2.23-, 2.07-, 2.44-, and 1.49-fold smaller than that of the PBS group, laser group, cholesterol group, and GDYO + laser + cholesterol group, respectively. However, we found that the treatment supplemented with cholesterol after PDT could slow down the fast growth trend of tumors compared to the PBS group, laser group and GDYO group. Yet, this inhibition effect was less pronounced than that of the GDYO + laser group (Figure 6C), and tumor images (Figure 6D) were in accord with the analysis of tumor weight (Figure 6E), highlighting that cholesterol levels modulate the anti-tumor effects. Furthermore, corresponding GDYO treatments should be identified and each potential toxic side effect must be eliminated prior to the initiation clinical trials. As illustrated in Figure 6B, the average body weights of mice in all of the groups receiving various treatments showed relatively small differences.

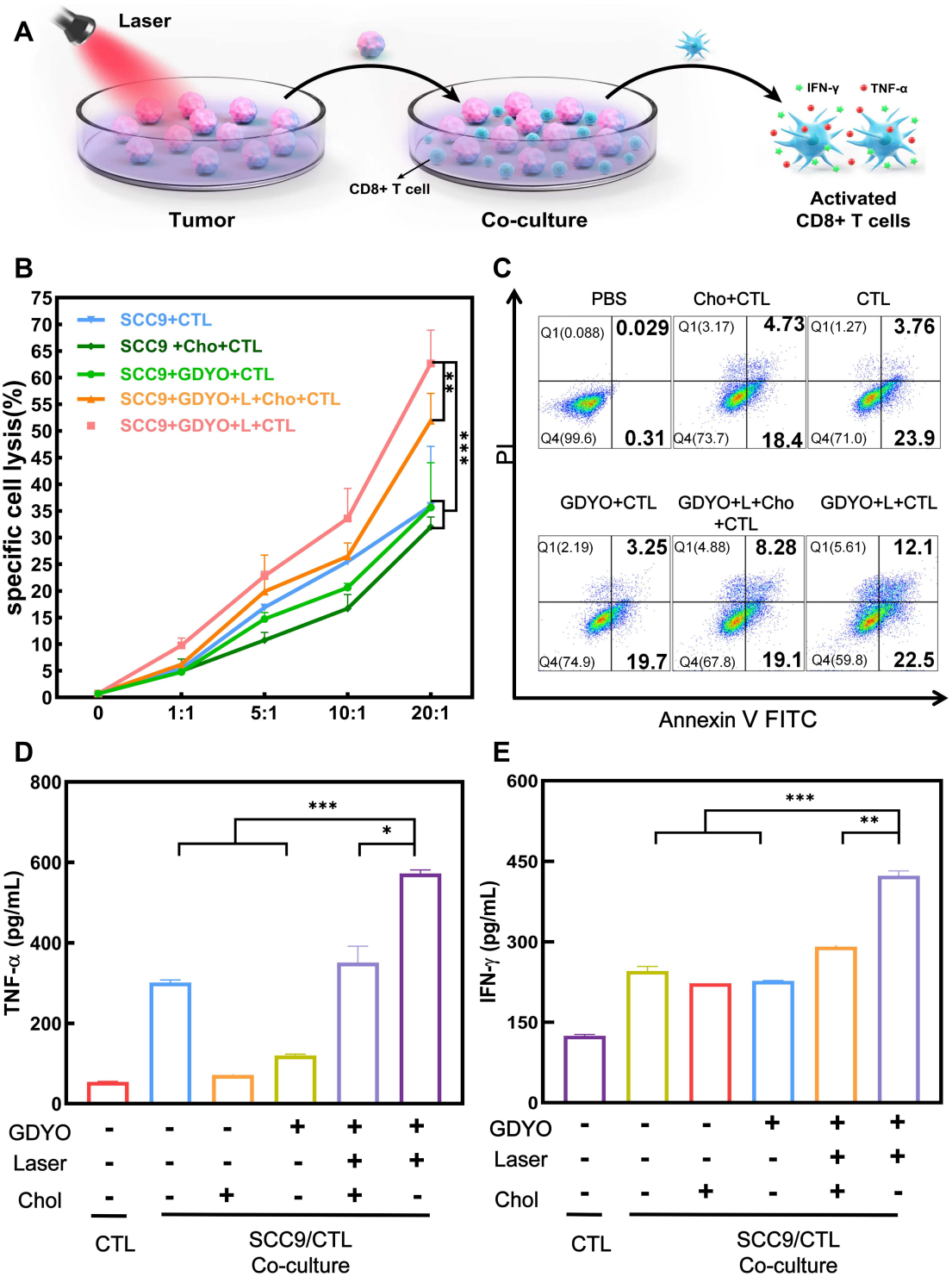

Figure 5 PDT enhances T lymphocytes activity. (**A**) Schematic illustration of the in vitro co-culture process of pre-treated SCC9 cells and activated T cells. (**B**) Activated CD8 T cells were co-cultured with PBS-treated, cholesterol-treated, GDYO-treated, GDYO-laser-treated and GDYO-laser-cholesterol-treated SCC9 cells (E:T ratio = 1:1, 5:1, 10:1, 20:1). Supernatant was used for LDH releasing assay. (**C**) The cell death mechanism was determined by assaying for apoptosis using an Annexin V-FITC/PI apoptosis kit (E:T ratio = 10:1). The release of (**D**) TNF-α and (**E**) IFN-γ cytokines production in the supernatant of the co-culture assay (E:T ratio=10:1) were detected using ELISA. *P <0.05, **P <0.01, ***P <0.001.

In view of the remarkable tumor inhibition effect of the GDYO + laser treatment, we further investigated the immune activation effect in mice with in situ OSCC tumors after different treatments. Considering the essential role of $CD8^+$ T cells in antitumor immunotherapy, the infiltration of $CD8^+$ T cells detected by immunofluorescent

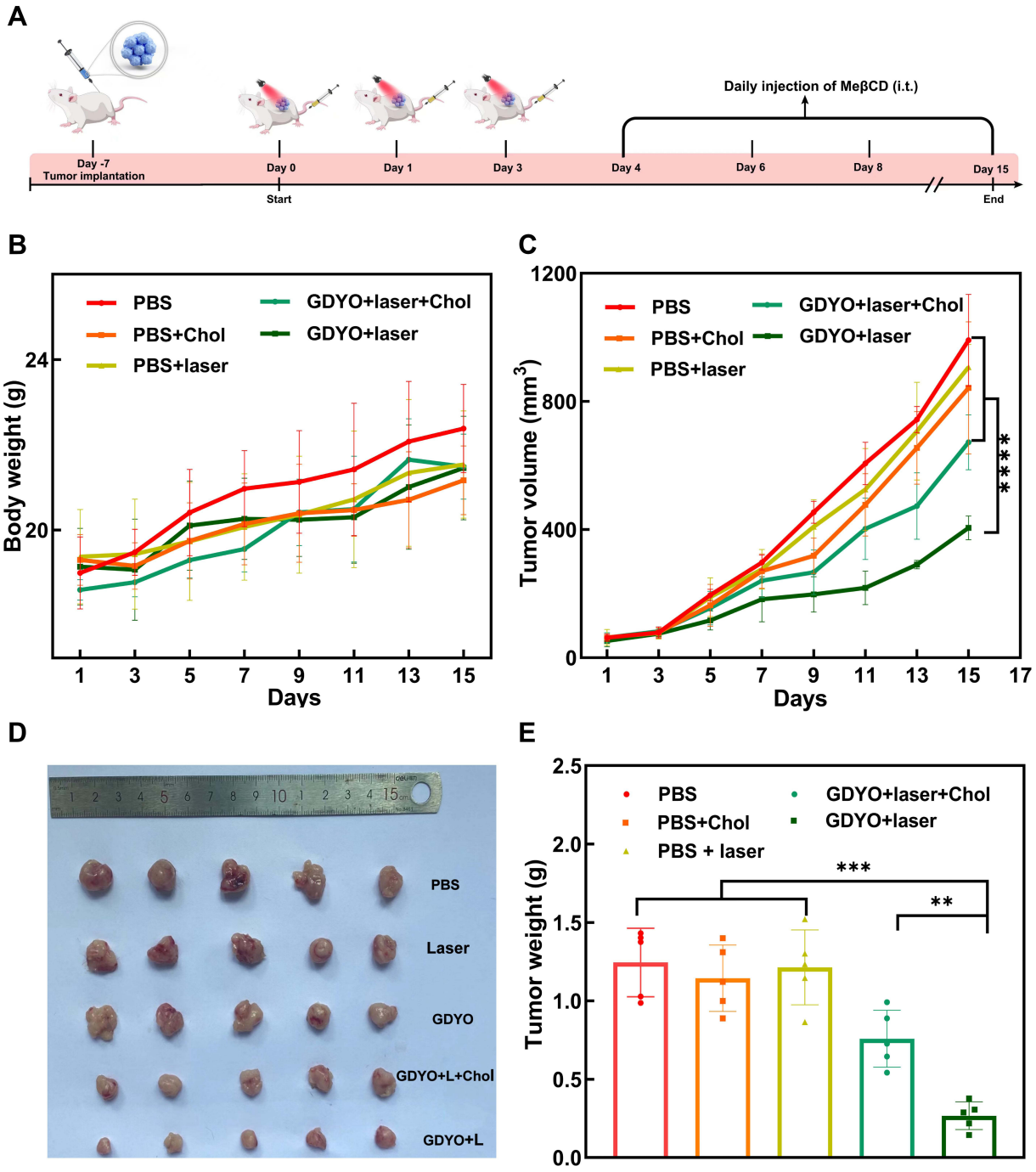

Figure 6 In vivo antitumor and therapeutic evaluation of GDYO. (**A**) Schematic illustration of the in vivo process. (**B**) Body weight variation in mice following various treatments. (**C**) Relative tumor volume study after multiple treatment. Tumor form (**D**) and weight (**E**) during treatment in each group. **P <0.01, ***P <0.001, ****P <0.0001.

staining of tumor tissues was the highest in the GDYO + laser group (Figure 7A), exhibiting an intensive immune response. The tumors were then assessed using flow cytometry. As expected, in the GDYO + laser group, the percentage of $CD8^+$ T cells (CD8 gated on CD3) increased significantly, and was 2.4-, 1.8-, 2.9-, and 1.3-fold higher than that of the PBS group, laser group, cholesterol group and GDYO + laser + cholesterol group, respectively (Figure 7B). Moreover, the amplified infiltration of IFN-γ and TNF-α, which act as inflammation factors indicating cytotoxicity of $CD8^+$ T cell-induced antitumor immunity[56] was measured in this study. Significantly higher elevation of IFN-γ and TNF-α (Figure 7D and Figure 7) secreted by CTLs in tumors were

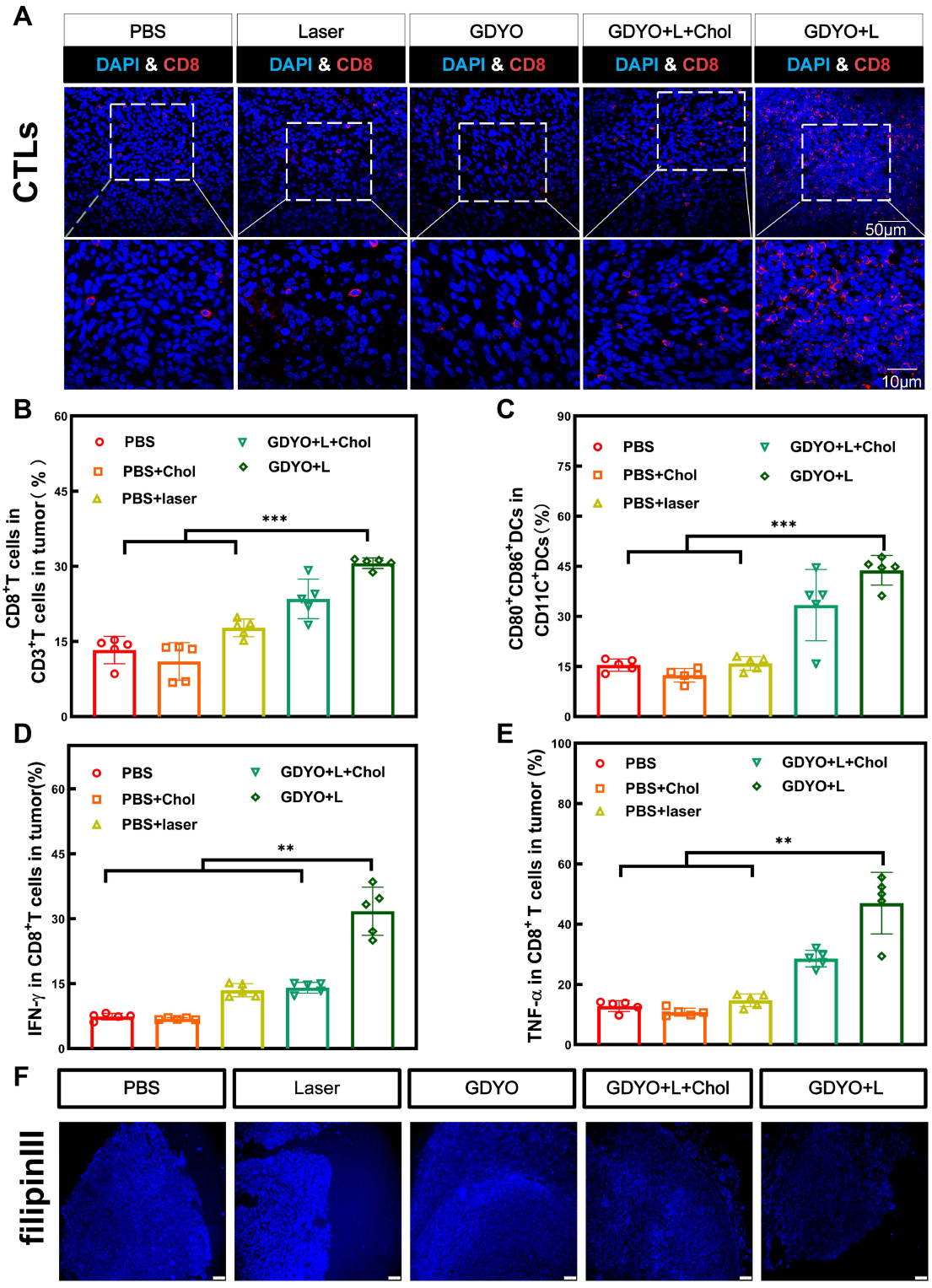

Figure 7 Assessment of intratumoral immune responses in vivo. (**A**) Representative immunofluorescent infiltration images of $CD8^+$ T cells in tumor sections of diverse groups. (**B**) Tumor mass normalized intratumoral infiltration of $CD8^+$ T cells. (**C**) DC maturation ratio in the LNs. (**D**) and (**E**) Expression analysis of IFN-γ^+ $CD8^+$ T cells and TNF-α^+ $CD8^+$ T cells in tumor tissues following different treatments. (**F**) Tumor tissues after different treatments were stained with Filipin III (shown in blue color). Scale bar =100 μm. **P <0.01, ***P <0.001.

observed after GDYO + laser treatment, indicating successful cellular immunity initiated by this approach. Given the fact that dendritic cells (DCs) are an essential part of the immune system linked to the development of T lymphocytes,[57] further investigation of the maturation of DCs (CD80, CD86 gated on CD11C) in tumor lymph

nodes were assessed and showed a significant boost of mature DCs, indicating that the GDYO + laser treatment could promote the antitumor effect (Figure 7C).

Moreover, it has been reported that membrane cholesterol levels correlate with cell stiffness, and decreased cholesterol from the cortical structure in cancer cells increases cell stiffness.[58,59] After various treatments, we collected tumor tissues to measure the cholesterol level by staining with Filipin III, which specifically binds to cholesterol. The results showed a substantially higher cholesterol level in the control groups (treated with PBS, laser, or GDYO only). However, no significant cholesterol was observed in the tumors of mice treated with GDYO and laser together (Figure 7F), indicating that cholesterol was downgraded after PDT treatment and played an inhibitory role in antitumor immunotherapy.

Together, these data highlight that as a result of the depletion of cholesterol in the treatment of GDYO with light irradiation, the mechanical characteristics of tumor cells were significantly decreased, thus boosting the $CD8^+$ T cell-mediated immune response and tumor killing in vivo.

Conclusion

Hence, the biophysical effects of increased cancer cell stiffness enhance its capacity to activate cytotoxic lymphocytes, which together with PDT-induced cell apoptosis not only assists in preventing tumor developmentbut also efficiently enhances the tumor immune microenvironment. A better understanding of the influence of GDYO photodynamic therapy on the mechanical softness of refractory tumor cells will provide a new and crucial foundation for the development of new nano-photosensitizers, which would influence the mechanical properties of cancer cells and would be suitable for immunotherapeutic strategies to improve patient responses to PDT.

Acknowledgments

This study was funded by the National Natural Science Foundation of China (No. 82073378 and No.81974746) and by the Open Fund of Guangdong Key Laboratory of Pharmaceutical Functional Genes (No. 2021A1515012399).

Disclosure

The authors have declared that no competing interests exist.

References

1. Ren ZH, Hu CY, He HR, Li YJ, Lyu J. Global and regional burdens of oral cancer from 1990 to 2017: results from the global burden of disease study. *Cancer Commun*. 2020;40(2–3):81–92. doi:10.1002/cac2.12009
2. Duan X, He C, Kron SJ, Lin W. Nanoparticle formulations of cisplatin for cancer therapy. *Wiley Interdiscip Rev Nanomed Nanobiotechnol*. 2016;8(5):776–791. doi:10.1002/wnan.1390
3. Boztepe T, Castro GR, Leon IE. Lipid, polymeric, inorganic-based drug delivery applications for platinum-based anticancer drugs. *Int J Pharmaceut*. 2021;605. doi:10.1016/j.ijpharm.2021.120788
4. Goldberg M, Manzi A, Conway P, et al. A nanoengineered topical transmucosal cisplatin delivery system induces anti-tumor response in animal models and patients with oral cancer. *Nat Commun*. 2022;13(1):4829. doi:10.1038/s41467-022-31859-3
5. Yamana K, Inoue J, Yoshida R, et al. Extracellular vesicles derived from radioresistant oral squamous cell carcinoma cells contribute to the acquisition of radioresistance via the miR-503-3p-BAK axis. *J Extracell Vesicles*. 2021;10(14):e12169. doi:10.1002/jev2.12169
6. Karan D, Holzbeierlein JM, Van Veldhuizen P, Thrasher JB. Cancer immunotherapy: a paradigm shift for prostate cancer treatment. *Nat Rev Urol*. 2012;9(7):376–385. doi:10.1038/nrurol.2012.106
7. Pauken KE, Dougan M, Rose NR, Lichtman AH, Sharpe AH. Adverse events following cancer immunotherapy: obstacles and opportunities. *Trends Immunol*. 2019;40(6):511–523. doi:10.1016/j.it.2019.04.002
8. Yu WQ, Sun JL, Wang XY, et al. Boosting cancer immunotherapy via the convenient A2AR inhibition using a tunable nanocatalyst with light-enhanced activity. *Adv Mater*. 2022;34:8. doi:10.1002/adma.202106967
9. Ribas A, Wolchok JD. Cancer immunotherapy using checkpoint blockade. *Science*. 2018;359(6382):1350. doi:10.1126/science.aar4060
10. Li G, Jiang Y, Qin Y, Yuan S, Chen X. Comparing development strategies for PD1/PDL1-based immunotherapies. *Nat Rev Drug Discov*. 2022;21(7):484. doi:10.1038/d41573-022-00003-7
11. Dolladille C, Ederhy S, Sassier M, et al. Immune checkpoint inhibitor rechallenge after immune-related adverse events in patients with cancer. *JAMA Oncol*. 2020;6(6):865–871. doi:10.1001/jamaoncol.2020.0726
12. Eil R, Vodnala SK, Clever D, et al. Ionic immune suppression within the tumour microenvironment limits T cell effector function. *Nature*. 2016;537(7621):539. doi:10.1038/nature19364
13. Andre P, Denis C, Soulas C, et al. Anti-NKG2A mAb is a checkpoint inhibitor that promotes anti-tumor immunity by unleashing both T and NK cells. *Cell*. 2018;175(7):1731. doi:10.1016/j.cell.2018.10.014
14. Alibert C, Goud B, Manneville JB. Are cancer cells really softer than normal cells?. *Biol Cell*. 2017;109(5):167–189. doi:10.1111/boc.201600078

15. Lv J, Liu Y, Cheng F, et al. Cell softness regulates tumorigenicity and stemness of cancer cells. *EMBO J*. 2021;40(2):e106123. doi:10.15252/embj.2020106123
16. Qin Y, Chen K, Gu W, et al. Small size fullerenol nanoparticles suppress lung metastasis of breast cancer cell by disrupting actin dynamics. *J Nanobiotechnology*. 2018;16(1):54. doi:10.1186/s12951-018-0380-z
17. Xu WW, Mezencev R, Kim B, Wang LJ, McDonald J, Sulchek T. Cell stiffness is a biomarker of the metastatic potential of ovarian cancer cells. *PLoS One*. 2012;7:10. doi:10.1371/journal.pone.0046609
18. Usmani SM, Mempel TR. Cancer cells relax and resist cytotoxic attack. *Immunity*. 2021;54(5):853–855. doi:10.1016/j.immuni.2021.04.017
19. Xie JL, Wang YW, Choi W, et al. Overcoming barriers in photodynamic therapy harnessing nano-formulation strategies. *Chem Soc Rev*. 2021;50(16):9152–9201. doi:10.1039/d0cs01370f
20. Xiao X, Liang S, Zhao YJ, et al. Multifunctional carbon monoxide nanogenerator as immunogenic cell death drugs with enhanced antitumor immunity and antimetastatic effect. *Biomaterials*. 2021:277. doi:10.1016/j.biomaterials.2021.121120
21. Hu X, Hou B, Xu Z, et al. Supramolecular prodrug nanovectors for active tumor targeting and combination immunotherapy of colorectal cancer. *Adv Sci*. 2020;7(8):1903332. doi:10.1002/advs.201903332
22. Fang Y, Liu YX, Qi L, Xue YR, Li YL. 2D graphdiyne: an emerging carbon material. *Chem Soc Rev*. 2022;51(7):2681–2709. doi:10.1039/d1cs00592h
23. Huang CS, Li YJ, Wang N, et al. Progress in research into 2D graphdiyne-based materials. *Chem Rev*. 2018;118(16):7744–7803. doi:10.1021/acs.chemrev.8b00288
24. Wang Q, Liu Y, Wang H, et al. Graphdiyne oxide nanosheets display selective anti-leukemia efficacy against DNMT3A-mutant AML cells. *Nat Commun*. 2022;13(1):5657. doi:10.1038/s41467-022-33410-w
25. Xie ZJ, Peng MH, Lu RT, et al. Black phosphorus-based photothermal therapy with aCD47-mediated immune checkpoint blockade for enhanced cancer immunotherapy. *Light Sci Appl*. 2020;9:1. doi:10.1038/s41377-020-00388-3
26. Yin F, Hu K, Chen S, et al. Black phosphorus quantum dot based novel siRNA delivery systems in human pluripotent teratoma PA-1 cells. *J Mater Chem B*. 2017;5(27):5433–5440. doi:10.1039/c7tb01068k
27. Xie ZJ, Chen SY, Duo YH, et al. Biocompatible two-dimensional titanium nanosheets for multimodal imaging-guided cancer theranostics. *Acs Appl Mater Inter*. 2019;11(25):22129–22140. doi:10.1021/acsami.9b04628
28. Xing CY, Chen SY, Liang X, et al. Two-dimensional MXene (Ti3C2)-Integrated cellulose hydrogels: toward smart three-dimensional network nanoplatforms exhibiting light-induced swelling and bimodal photothermal/chemotherapy anticancer activity. *Acs Appl Mater Inter*. 2018;10(33):27631–27643. doi:10.1021/acsami.8b08314
29. Xing CY, Chen SY, Qiu M, et al. Conceptually novel black phosphorus/cellulose hydrogels as promising photothermal agents for effective cancer therapy. *Adv Healthc Mater*. 2018;7(7). doi:10.1002/adhm.201701510
30. Jiang W, Zhang Z, Wang Q, et al. Tumor reoxygenation and blood perfusion enhanced photodynamic therapy using ultrathin graphdiyne oxide nanosheets. *Nano Lett*. 2019;19(6):4060–4067. doi:10.1021/acs.nanolett.9b01458
31. Xing EY, Du YY, Yin JJ, et al. Multi-functional nanodrug based on a three-dimensional framework for targeted photo-chemo synergetic cancer therapy. *Adv Healthc Mater*. 2021;10:8. doi:10.1002/adhm.202001874
32. Guo M, Zhao L, Liu J, et al. The underlying function and structural organization of the intracellular protein corona on graphdiyne oxide nanosheet for local immunomodulation. *Nano Lett*. 2021;21(14):6005–6013. doi:10.1021/acs.nanolett.1c01048
33. Peng G, Duan T, Guo M, et al. Biodegradation of graphdiyne oxide in classically activated (M1) macrophages modulates cytokine production. *Nanoscale*. 2021;13(30):13072–13084. doi:10.1039/d1nr02473f
34. Zhang D, Feng F, Li Q, Wang X, Yao L. Nanopurpurin-based photodynamic therapy destructs extracellular matrix against intractable tumor metastasis. *Biomaterials*. 2018;173:22–33. doi:10.1016/j.biomaterials.2018.04.045
35. Liu T, Wu LY, Berkman CE. Prostate-specific membrane antigen-targeted photodynamic therapy induces rapid cytoskeletal disruption. *Cancer Lett*. 2010;296(1):106–112. doi:10.1016/j.canlet.2010.04.003
36. Yan H, Guo S, Wu F, et al. Carbon atom hybridization matters: ultrafast humidity response of graphdiyne oxides. *Angew Chem Int Ed Engl*. 2018;57(15):3922–3926. doi:10.1002/anie.201709417
37. Xing E, Du Y, Yin J, et al. Multi-functional nanodrug based on a three-dimensional framework for targeted photo-chemo synergetic cancer therapy. *Adv Healthc Mater*. 2021;10(8):e2001874. doi:10.1002/adhm.202001874
38. Ma W, Xue Y, Guo S, et al. Graphdiyne oxide: a new carbon nanozyme. *Chem Commun*. 2020;56(38):5115–5118. doi:10.1039/d0cc01840f
39. Wang YW, Qiu M, Won M, et al. Emerging 2D material-based nanocarrier for cancer therapy beyond graphene. *Coordin Chem Rev*. 2019:400. doi:10.1016/j.ccr.2019.213041
40. Zhu Y, Xie ZJ, Li JF, et al. From phosphorus to phosphorene: applications in disease theranostics. *Coordin Chem Rev*. 2021:446. doi:10.1016/j.ccr.2021.214110
41. Calzado-Martin A, Encinar M, Tamayo J, Calleja M, San Paulo A. Effect of actin organization on the stiffness of living breast cancer cells revealed by peak-force modulation atomic force microscopy. *ACS Nano*. 2016;10(3):3365–3374. doi:10.1021/acsnano.5b07162
42. Handel C, Schmidt BUS, Schiller J, et al. Cell membrane softening in human breast and cervical cancer cells. *New J Phys*. 2015:17. doi:10.1088/1367-2630/17/8/083008
43. Malohlava J, Tomankova K, Malina L, et al. Effect of porphyrin sensitizer MgTPPS4 on cytoskeletal system of hela cell line-microscopic study. *Cell Biochem Biophys*. 2016;74(3):419–425. doi:10.1007/s12013-016-0746-5
44. Pi J, Cai HH, Jin H, et al. Qualitative and quantitative analysis of ROS-mediated oridonin-induced oesophageal cancer KYSE-150 cell apoptosis by atomic force microscopy. *PLoS One*. 2015;10:10. doi:10.1371/journal.pone.0140935
45. Misiak P, Niemirowicz-Laskowska K, Markiewicz KH, et al. Evaluation of cytotoxic effect of cholesterol End-capped Poly(N-isopropylacrylamide) s on selected normal and neoplastic cells. *Int J Nanomed*. 2020;15:7263–7278. doi:10.2147/Ijn.S262582
46. Maja M, Mohammed D, Dumitru AC, et al. Surface cholesterol-enriched domains specifically promote invasion of breast cancer cell lines by controlling invadopodia and extracellular matrix degradation. *Cell Mol Life Sci*. 2022;79(8):417. doi:10.1007/s00018-022-04426-8
47. Ma X, Bi E, Lu Y, et al. Cholesterol induces CD8(+) T cell exhaustion in the tumor microenvironment. *Cell Metab*. 2019;30(1):143–56e5. doi:10.1016/j.cmet.2019.04.002

48. Greenlee JD, Subramanian T, Liu K, King MR. Rafting down the metastatic cascade: the role of lipid rafts in cancer metastasis, cell death, and clinical outcomes. *Cancer Res*. 2021;81(1):5–17. doi:10.1158/0008-5472.CAN-20-2199
49. Zhang L, Xu B, Wang X. Cholesterol extraction from cell membrane by graphene nanosheets: a computational study. *J Phys Chem B*. 2016;120 (5):957–964. doi:10.1021/acs.jpcb.5b10330
50. Gu ZL, Yang ZX, Luan BQ, et al. Membrane insertion and phospholipids extraction by graphyne nanosheets. *J Phys Chem C*. 2017;121 (4):2444–2450. doi:10.1021/acs.jpcc.6b10548
51. Taninaka A, Ugajin S, Kurokawa H, et al. Direct analysis of the actin-filament formation effect in photodynamic therapy. *RSC Adv*. 2022;12 (10):5878–5889. doi:10.1039/d1ra09291j
52. Basu R, Whitlock BM, Husson J, et al. Cytotoxic T cells use mechanical force to potentiate target cell killing. *Cell*. 2016;165(1):100–110. doi:10.1016/j.cell.2016.01.021
53. Rudzka DA, Spennati G, McGarry DJ, et al. Migration through physical constraints is enabled by MAPK-induced cell softening via actin cytoskeleton re-organization. *J Cell Sci*. 2019;132(11). doi:10.1242/jcs.224071
54. Kammertoens T, Friese C, Arina A, et al. Tumour ischaemia by interferon-gamma resembles physiological blood vessel regression. *Nature*. 2017;545(7652):98–102. doi:10.1038/nature22311
55. Zhang XL, Li HY, Yi C, et al. Host immune response triggered by graphene quantum-dot-mediated photodynamic therapy for oral squamous cell carcinoma. *Int J Nanomed*. 2020;15:9627–9638. doi:10.2147/Ijn.S276153
56. Wang YQ, Zhao ZL, Liu CL, et al. B16 membrane-coated vesicles for combined photodynamic therapy and immunotherapy shift immune microenvironment of melanoma. *Int J Nanomed*. 2022;17:855–868. doi:10.2147/Ijn.S338488
57. Ou W, Jiang L, Thapa RK, et al. Combination of NIR therapy and regulatory T cell modulation using layer-by-layer hybrid nanoparticles for effective cancer photoimmunotherapy. *Theranostics*. 2018;8(17):4574–4590. doi:10.7150/thno.26758
58. Byfield FJ, Aranda-Espinoza H, Romanenko VG, Rothblat GH, Levitan I. Cholesterol depletion increases membrane stiffness of aortic endothelial cells. *Biophys J*. 2004;87(5):3336–3343. doi:10.1529/biophysj.104.040634
59. Khatibzadeh N, Gupta S, Farrell B, Brownell WE, Anvari B. Effects of cholesterol on nano-mechanical properties of the living cell plasma membrane. *Soft Matter*. 2012;8(32):8350–8360. doi:10.1039/C2SM25263E